



This is a repository copy of *Solidification and stabilization of strontium and chloride ions in thermally treated calcium aluminate cement modified with or without sodium polyphosphate*.

White Rose Research Online URL for this paper:

<https://eprints.whiterose.ac.uk/184641/>

Version: Accepted Version

---

**Article:**

Irisawa, K., Namiki, M., Taniguchi, T. et al. (2 more authors) (2022) Solidification and stabilization of strontium and chloride ions in thermally treated calcium aluminate cement modified with or without sodium polyphosphate. *Cement and Concrete Research*, 156. 106758. ISSN 0008-8846

<https://doi.org/10.1016/j.cemconres.2022.106758>

---

Article available under the terms of the CC-BY-NC-ND licence (<https://creativecommons.org/licenses/by-nc-nd/4.0/>).

**Reuse**

This article is distributed under the terms of the Creative Commons Attribution-NonCommercial-NoDerivs (CC BY-NC-ND) licence. This licence only allows you to download this work and share it with others as long as you credit the authors, but you can't change the article in any way or use it commercially. More information and the full terms of the licence here: <https://creativecommons.org/licenses/>

**Takedown**

If you consider content in White Rose Research Online to be in breach of UK law, please notify us by emailing [eprints@whiterose.ac.uk](mailto:eprints@whiterose.ac.uk) including the URL of the record and the reason for the withdrawal request.



[eprints@whiterose.ac.uk](mailto:eprints@whiterose.ac.uk)  
<https://eprints.whiterose.ac.uk/>

**Solidification and stabilization of strontium and chloride ions in thermally treated calcium aluminate cement modified with or without sodium polyphosphate**

Keita Irisawa<sup>a,b</sup>, Masahiro Namiki<sup>c</sup>, Takumi Taniguchi<sup>a</sup>, Inés Garcia-Lodeiro<sup>d,e</sup>, Hajime Kinoshita<sup>d</sup>

<sup>a</sup> Sector of Nuclear Fuel, Decommissioning and Waste Management Technology Development, Japan Atomic Energy Agency, Tokai, Japan.

<sup>b</sup> National Institute of Technology (KOSEN), Ibaraki College, Ibaraki, Japan.

<sup>c</sup> Inspection Development Company Ltd., Tokai, Japan.

<sup>d</sup> Department of Materials Science and Engineering, The University of Sheffield, Sheffield, UK.

<sup>e</sup> Department of Materials, Eduardo Torroja Institute (IETcc-CSIC), Madrid, Spain.

Corresponding author

Keita Irisawa

E-mail: [kirisawa@ibaraki-ct.ac.jp](mailto:kirisawa@ibaraki-ct.ac.jp)

Tel: +81-29-271-2990

Fax: +81-29-271-2992

Permanent address: 866 Nakane, Hitachinaka, Ibaraki 312-8508, Japan

## Abstract

Cementation of aqueous radioactive waste contaminated with a significant  $^{90}\text{Sr}$  is challenging due to the potential radiolysis of water contents. Utilization of calcium aluminate cement (CAC) modified with sodium polyphosphate (CAP) is interesting as its water content can be reduced by thermal treatment. The present study investigated solidification and stabilization of  $\text{Sr}^{2+}$  and  $\text{Cl}^-$  ions in CAC and CAP with or without thermal treatment. A leaching test showed a superior  $\text{Sr}^{2+}$  ion stabilization in CAP: apparent diffusion coefficient of  $\text{Sr}^{2+}$  was smaller than in the CAC by 5 orders of magnitude. CAC cured at 20 °C had the best stabilization for  $\text{Cl}^-$  ions among the samples tested. Friedel's salt formed in CAC may have contributed to the immobilization of  $\text{Cl}^-$  ions. The stabilization of  $\text{Cl}^-$  ions by CAP was significantly improved by the thermal treatment likely because of the improvement in the microstructure previously reported.

(145 words)

## Keywords

Calcium aluminate cement, sodium polyphosphate, strontium, chloride, thermal treatment

## 1. Introduction

### 1.1. Background

The Fukushima Daiichi nuclear power station disaster and associated clean-up process generate a large volume of aqueous secondary wastes. Those from the contaminated water treatment often contain radionuclides (mainly strontium-90 [1]), sea salts (e.g.,  $\text{Na}^+$  and  $\text{Cl}^-$  ions [2]) and a large water content. Strontium-90 ( $^{90}\text{Sr}$ ), decays by a  $\beta$ -ray emission with a half-life of 28.8 years, is one of the most important nuclear fission products. Aqueous secondary wastes contaminated with a significant  $^{90}\text{Sr}$  may lead to the radiolysis of the water component, resulting in hydrogen gas generation. A long-term storage of the aqueous secondary wastes would face the potential risks of not only leakage into the environment but also of fire and explosion due to the accumulation of radiolytic  $\text{H}_2$  gas. Hence, conversion of such wastes to a suitable and stable form would be effective to minimize these risks.

Radioactive wastes of this type can usually be encapsulated in the cementing grouts based on ordinary Portland cement (PC). However, for this particular secondary waste, cementation by the conventional PC-based matrices is challenging because the risk of  $\text{H}_2$  gas would remain due to the radiolysis of the water content intrinsically exists as the pore solution and the hydrated phases.

### 1.2. CAC and CAP cement

Present investigation focuses on calcium aluminate cement (CAC) and CAC modified with phosphate (CAP). CAC is one of the alternative cements to PC, a well-known material that has been used to solidify and encapsulate radioactive wastes [3], commonly blended with supplemental cementitious materials such as blast furnace slag or fly ash. One of the characteristics in CAC is that the internal environment has a significantly lower pH (10.5-11 [4]) than that in PC and its blended systems (>13 [5]). By utilizing this characteristic, encapsulation of the reactive metallic radioactive wastes in CAC has been investigated [5]. Modification of CAC with phosphate (CAP) can further reduce the pH (9.0-10.5 [5]). The modification of CAC by phosphate is also known to prevent the conventional hydration of CAC, and results in solidification via an acid-base reaction between acidic phosphate solution and CAC powders acting as a base [6-12]. Owing to its characteristic solidification reaction and/or the internal low pH environment, CAP has been investigated in recent years for solidification and stabilization of hazardous and radioactive materials [13-17].

### 1.3. Focus of the study

The CAP system, especially thermally treated CAP is interesting because it has been reported that hydroxyapatite,  $\text{Ca}_{10}(\text{PO}_4)_6(\text{OH})_2$ , and related amorphous phosphate phases could be formed, and water content (capillary water and gel water) reduced in the system [16,17]. The thermally treated CAP may be expected to have a good immobilization capability of  $\text{Sr}^{2+}$  and  $\text{Cl}^-$  ions since the apatite family of calcium phosphates is known to be a good host for Sr and halogens [18]. In addition, a

smaller water content minimized by thermal treatment leads to the reduced risk of radiolytic H<sub>2</sub> gas generation. It has been reported that the rate of H<sub>2</sub> gas generation upon irradiation of concrete decreases with the decrease in the evaporable water such as capillary water and gel water [19].

The present study, therefore, investigated the solidification and stabilization of Sr<sup>2+</sup> and Cl<sup>-</sup> ions in the CAC and the CAP systems, focusing on the leaching behavior these ions from the produced cement systems, aiming for their applications as the encapsulant for waste immobilization. The CAC and CAP systems were synthesized by mixing SrCl<sub>2</sub> aqueous solution and CAC with or without sodium polyphosphate powders. This was followed by curing in an open system at 90 °C, or in a closed system at 20 °C as a reference. Leaching tests for both the CAC and CAP systems were undertaken based on ANSI/ANS16.1 [18], as commonly used for nuclear wasteforms.

## 2. Experimental

### 2.1. Synthesis of samples

Secar<sup>®</sup>51 (>50 wt% Al<sub>2</sub>O<sub>3</sub>, <39.5 wt% CaO, <6.0 wt% SiO<sub>2</sub>, <4.0 wt% TiO<sub>2</sub>), supplied by Kerneos Ltd., was used as calcium aluminate cement. A mixing solution, in which the concentration of Sr<sup>2+</sup> and Cl<sup>-</sup> were 5.0 × 10<sup>5</sup> µg/mL and 4.2 × 10<sup>5</sup> µg/mL, respectively, was prepared by dissolution of strontium chloride, SrCl<sub>2</sub>·6H<sub>2</sub>O (99%, Fujifilm Wako Pure Chemical Corporation) in deionized water of 18.2 MΩ. For the CAC sample, 100 g of Secar<sup>®</sup>51 was used as a binder, while for the CAP sample, 100 g of Secar<sup>®</sup>51 and 40 g of sodium polyphosphate, (NaPO<sub>3</sub>)<sub>n</sub> (65-70%, Acros Organics Ltd.), were manually homogenized prior to the introduction of the mixing solution. The mixing solution of 35 mL was added into the powders (CAC or a mixture of CAC and (NaPO<sub>3</sub>)<sub>n</sub>), then manually mixed for 30 seconds and mechanically for 120 seconds by a high share mixer (L5MA, Silverson Co.) at 2500 rpm. The CAC and the CAP pastes were put into 50 mL plastic tubes, followed by 1 minute of vibration. The caps for some of tubes were screwed on tightly and then sealed by Parafilm<sup>®</sup>. The sealed tubes were cured as closed system for 7 days at 20 °C in a constant temperature container as a reference (CAC<sub>20</sub>, CAP<sub>20</sub>). The other tubes, without their caps, were cured in an open system for the same period at 90 °C in an oven (CAC<sub>90</sub>, CAP<sub>90</sub>), based on the curing condition of the previous studies [16,17]. During the curing, the weights of the samples were monitored. After the curing, the samples were cut for a leaching test and analysis. A small part of the samples were crushed and sieved to less than 63 µm, and were used for x-ray diffractometry (XRD, Ultima IV, Rigaku Co.), thermogravimetry analysis (TG and DTG, TG/DTA7200, Hitachi High-Tech Co.) and attenuated total reflectance Fourier transform infrared spectroscopy (ATR/FT-IR, ATRPRO670H-S, FT/IR 4000, Jasco Co.). X-ray diffractograms was scanned in the 2θ range from 5° to 55° with a step size of 0.02° and at a rate of 1°/min. Thermogravimetry analysis was also carried out, in an aluminum crucible with powdered samples heated from room temperature to 500 °C at a rate of 10 °C/min in a N<sub>2</sub> flow (200 cm<sup>3</sup>/min).

## 2.2. Leaching test

The sample sizes (25.5 mm $\phi$   $\times$  10 mmH) were used for a leaching test (surface area:  $\sim$ 18 cm<sup>2</sup>). The deionized water (volume:  $\sim$ 180 mL) was used as a leachate. A ratio of leachate volume to the specimen external geometric surface area is  $10.0 \pm 0.1$  cm. A vessel for the leaching test was a 250 mL polyethylene vessel (63 mm $\phi$   $\times$  120 mmH). Leaching temperature was kept at 20 °C in a constant temperature container. The leachate was not stirred, and was replaced at the set leaching intervals (2 h, 7 h, 24 h, 2 d, 3 d, 4 d, 14 d, 28 d, 43 d, 91 d). The concentrations of Sr<sup>2+</sup> and Cl<sup>-</sup> in the leachates were measured by inductivity coupled plasma-optical emission spectrometry (ICP-OES, ICP-8000E, Shimadzu Ltd.) and ion chromatography (ICS-1000, Dionex Ltd.), respectively. The cumulative fraction leached (CFL) in the leaching test was calculated for Sr and Cl ions using Eq. 1.

$$(\text{CFL}) = \frac{A_t}{A_0} = \frac{1}{A_0} \sum_i c_i \times V_{L,i} \quad (1)$$

where  $A_t$  is the cumulative mass of the Sr<sup>2+</sup> or Cl<sup>-</sup> leached out (mg),  $A_0$  is the total mass of the substance contained in the sample prior to the test (mg),  $c_i$  is the measured concentration of the leached Sr<sup>2+</sup> or Cl<sup>-</sup> in the leachate at the  $i$ -th leaching interval (mg/L) and  $V_{L,i}$  is the volume of the leachate (L). The plot of CFL against square root of time ( $t^{1/2}$ ) also enables the estimation of diffusion coefficients ( $D_e$ ) of Sr or Cl ions in the cement sample using Eq. 2 [20].

$$(\text{CFL}) = \frac{2S}{V} \sqrt{\frac{D_e t}{\pi}} \quad (2)$$

where  $S$  is the surface area of the sample (m<sup>2</sup>) used in the leaching test,  $V$  is the volume of the sample (m<sup>3</sup>),  $D_e$  is the diffusion coefficient (m<sup>2</sup>/s) and  $t$  is the leaching period (s). The samples were recovered after 91 days of leaching, wiped and powdered for analysis. CAC<sub>20</sub>, CAC<sub>90</sub>, CAP<sub>20</sub> and CAP<sub>90</sub> after 91 days leaching tests were named as CAC<sub>20A</sub>, CAC<sub>90A</sub>, CAP<sub>20A</sub> and CAP<sub>90A</sub>, respectively. Samples were also analyzed prior to the leaching test.

## 3. Results and discussion

### 3.1. Reduction of water

The weight of samples decreased during the curing period at 90 °C in the CAC<sub>90</sub> and the CAP<sub>90</sub>. Assuming the weight losses represent the evaporation of water from the CAC<sub>90</sub> and the CAP<sub>90</sub>, the water content remaining in the sample could be estimated as the following;

$$(\text{Remaining water content}) = \frac{W_0 - W_t}{W_0} \times 100 \quad (3)$$

where  $W_0$  is the initial weigh of water in the sample and  $W_t$  is weight loss of the sample due to water

evaporation recorded at a certain curing period. **Figure 1** shows remaining water contents (wt%) in CAC<sub>20</sub>, CAC<sub>90</sub>, CAP<sub>20</sub> and CAP<sub>90</sub> during the initial 7 days of curing. The water contents in the CAC<sub>20</sub> and the CAP<sub>20</sub> did not change, because they were closed system prepared as a reference case. The reduction of water content in the CAC<sub>90</sub> mostly took place during the first 24 h, and little reduction in the water content was observed after this period. On the other hand, water content in the CAP<sub>90</sub> gently decreased during the curing period. The obtained data for the CAC<sub>90</sub> and CAP<sub>90</sub> samples were consistent with those previously reported [16,17]. The remaining water content at the 7<sup>th</sup> day were approximately 64 wt% in the CAC<sub>90</sub> and 41 wt% in the CAP<sub>90</sub> compared with their initial water content, suggesting the reduction of water content by 36 wt% and 59 wt%, respectively. **These values correspond to the change in the water to cement (CAC) ratio from 0.35 in the original pastes to 0.22 CAC<sub>90</sub> and 0.14 for CAP<sub>90</sub>.**

### 3.2. Leaching behavior of Sr<sup>2+</sup>

**Figure 2** shows CFL of Sr<sup>2+</sup> in CAC<sub>20</sub>, CAC<sub>90</sub>, CAP<sub>20</sub> and CAP<sub>90</sub> against time (days). A significant leaching of Sr is observable in the CAC systems, indicating ~9% of leaching, whereas the leaching of Sr appears to be highly limited in the CAP systems. The leaching behavior of Sr<sup>2+</sup> from the CAC systems indicated a change at around 4 days. Similar behavior of Sr<sup>2+</sup> leaching has been observed in the PC-based systems [21-23]. The thermal treatment on CAC system appears to have increased the leaching of Sr slightly at the earlier stage, although overall leaching was reduced.

The CFL data are plotted against a square root of time (s<sup>1/2</sup>) in **Figure 3 (a) and (b)**. It should be noted that the scale of the vertical axis in **Figure 3 (b)** is much smaller than that in **Figure 3 (a)**. As previously mentioned, this plot allows us to determine the coefficient ( $D_e$ ) of Sr<sup>2+</sup> in the system based on Eq. 2. By examining the gradient of the data points,  $(CFL)/\sqrt{t}$ , in **Figure 3**, it is possible to estimate  $D_e$  using Eq. 4.

$$D_e = \pi \left\{ \frac{V}{2S} \right\}^2 \left\{ \frac{(CFL)}{\sqrt{t}} \right\}^2 \quad (4)$$

The CFL of Sr<sup>2+</sup> both in the CAC and the CAP systems proportionally increase with the square root of time up to the 4<sup>th</sup> day (approximately 588 s<sup>1/2</sup>), and then deviate from it. In **Figure 3 (b)**, it is also observed that the thermal treatment on the CAP system is effective to reduce the leaching of Sr<sup>2+</sup>. The outcomes of the analysis are summarized in **Table 1**. The gradient of the data,  $(CFL)/\sqrt{t}$  in the early leaching period, were obtained by the least-squares regression using the CFL data points, with a good correlation (*i.e.*,  $R^2 > 0.95$ ). The diffusion coefficients of Sr<sup>2+</sup> in CAP systems studied are smaller than that in the CAC system roughly by five order of magnitude. The very small  $D_e$  values of Sr<sup>2+</sup> in the CAP<sub>20</sub> and the CAP<sub>90</sub> systems implies that Sr<sup>2+</sup> existed in the system as a solid form with limited solubility.

### 3.3. Leaching behavior of $Cl^-$

CFL of  $Cl^-$  in CAC<sub>20</sub>, CAC<sub>90</sub>, CAP<sub>20</sub> and CAP<sub>90</sub> against time (days) are shown in **Figure 4**. Differing from  $Sr^{2+}$ , the leaching of  $Cl^-$  was less in the CAC system. For the CAC system, the effect of thermal treatment was also different, resulting in a significant increase in the leaching of  $Cl^-$ . On the other hand, the thermal treatment was effective for the CAP system to reduce the leaching of  $Cl^-$ . The change in the leaching behavior was also observed for  $Cl^-$  at around 4 days. The diffusion coefficient of  $Cl^-$  in the CAC and CAP systems are examined based on the gradient of the data,  $(CFL)/\sqrt{t}$  in the early leaching period shown in **Figure 5**. The outcomes of the analysis are shown in **Table 1**. Diffusion of  $Cl^-$  ions increased by the thermal treatment in the CAC system by one order of magnitude, clarifying the negative effect of thermal treatment for the retention of  $Cl^-$  in CAC. For the CAP system, the  $D_e$  value of  $Cl^-$  became roughly 1/3 by the thermal treatment.

### 3.4. Crystalline phase identification

**Figure 6** shows X-ray diffractograms (XRD) for the CAC and the CAP (a) prior and (b) subsequent to the leaching test. The XRD for the CAC<sub>20</sub> prior to the leaching test (**Figure 6(a)**) showed the crystalline CAC clinker phases; monocalcium aluminate (m: CA or  $CaAl_2O_4$ ), gehlenite (g:  $C_2AS$  or  $Ca_2Al_2SiO_7$ ), and perovskite (p: CT or  $CaTiO_3$ ) as well as the metastable hexagonal CAC hydration phase; monocalcium aluminate decahydrate (D:  $CAH_{10}$  or  $CaAl_2O_4 \cdot 10H_2O$ ). On the other hand, the CAC<sub>90</sub> prior to the leaching test showed stable CAC hydration phases, hydrogarnet (H:  $C_3AH_6$  or  $Ca_3Al_2O_6 \cdot 6H_2O$ ) and gibbsite (G:  $AH_3$  or  $Al(OH)_3$ ). In the both CAC systems, a reflection peak corresponding to Friedel's salt (F:  $3CaO \cdot Al_2O_3 \cdot CaCl_2 \cdot 10H_2O$ ) was observed at  $\sim 11^\circ$  ( $2\theta$ ). The formation of metastable crystalline hydration products ( $CAH_{10}$ ) at the ambient temperature and the stable phases ( $C_3AH_6$  and  $AH_3$ ) at the high temperature is consistent with the reported hydration behavior of CAC [24]. The Friedel's salt includes  $Cl^-$  ion in its crystal structure and is well known to immobilize  $Cl^-$  ion [25]. It was probably the reason for the CAC system to have a lower  $D_e$  value of  $Cl^-$ .

The XRD data of the CAC<sub>20A</sub> and the CAC<sub>90A</sub> in the **Figure 6 (b)** showed the same phases as those prior to the leaching test, except for dicalcium aluminate octahydrates (O:  $C_2AH_8$  or  $2CaO \cdot A_2O_3 \cdot 8H_2O$ ) formed in the CAC<sub>90A</sub>.  $C_2AH_8$  is another metastable CAC hydration phase similar to  $CAH_{10}$ . The formation of  $C_2AH_8$  suggests the conventional hydration of CAC clinker phases presented in the system by contacting with leachate during the 91 days of leaching test.

The XRD data for the CAP<sub>20</sub> and CAP<sub>90</sub> systems show no obvious reflection for either the CAC hydration products or any other crystalline phases other than the anhydrous clinker phases. The phosphate modification was altering the reaction pathway, preventing the conventional CAC hydration. The XRD data of CAP<sub>20A</sub> and CAP<sub>90A</sub> show no obvious difference from those prior to the leaching test, indicating that 91 days leaching did not make crystalline phases to form in the CAP system.

In the CAP systems, there is a possible peak for the hydroxyapatite at  $\sim 32^\circ$  ( $2\theta$ ) in **Figure 6 (a)**. Although it is difficult to assert its presence solely based on these data, according to the previous study [16], thermal treatment of CAP system can enhance the formation of poorly crystallized hydroxyapatite. The CFL of  $\text{Cl}^-$  for the CAP<sub>90</sub> was lower than that in the CAP<sub>20</sub>. These may suggest, assuming  $\text{Cl}^-$  did not escape by evaporation of water in the CAP<sub>90</sub>, that the poorly crystallized hydroxyapatite was incorporating  $\text{Cl}^-$  ion through the substitution of  $\text{Cl}^-$  with  $\text{OH}^-$  in its structure. The stabilization of  $\text{Cl}^-$  in the poorly crystallized hydroxyapatite appears to be less effective compared with the Friedel's salt in the CAC system according to the leaching data.

### 3.5. Evolution of phases

**Figure 7** shows TG and differential TG (DTG) data for the CAC systems against temperature. The TG and DTG show several weight loss events emphasized in DTG curves. They are useful to identify the evolution of phases after the leaching test. The main weight loss peaked at below 100 °C in CAC<sub>20</sub> and CAC<sub>20A</sub> represent weakly bound water of the amorphous gels such as hydrated alumina gel or a calcium aluminate hydrate (C-A-H) type gel [11]. CAH<sub>10</sub> was reported to dehydrate at the temperature of 120 °C, and the C<sub>2</sub>AH<sub>8</sub> dehydrates at  $\sim 200$  °C [26], but overlapping of the peaks in DTG makes it difficult to clearly assign the weight loss events. The small weight loss events in the region of 220 – 330 °C corresponds to the dehydration of gibbsite AH<sub>3</sub> [27] and hydrogarnet C<sub>3</sub>AH<sub>6</sub>, respectively [11]. The main weight losses corresponding to amorphous gels and CAH<sub>10</sub> observed in the CAC<sub>20</sub> appear to be increased in the CAC<sub>20A</sub>, as well as those at 220 – 300 °C attributed to AH<sub>3</sub> and C<sub>3</sub>AH<sub>6</sub>, indicating the further hydration of CAC clinkers that took place during the leaching test by interacting with the leachate.

On the other hand, the weight losses for the amorphous gels was very small in the CAC<sub>90</sub>, meaning that thermal treatment of the sample could evaporate free water and weakly bound water of the amorphous gels. This result confirms that thermal treatment was effective for removal of free water in the CAC. The weight losses at 220 – 330 °C corresponding to AH<sub>3</sub> and C<sub>3</sub>AH<sub>6</sub> are slightly enhanced in CAC<sub>90A</sub> in addition to those below 200 °C. These results confirm the further hydration of CAC clinker phases during the leaching test suggested by the XRD analysis.

**Figure 8** shows TG and DTG data for the CAP against temperature. With respect to the CAP<sub>20</sub>, the main weight loss was observed below 150 °C as a broad peak in the DTG curve, which could correspond to the loss of free water, as well as the loss of water loosely bonded with the amorphous sodium calcium orthophosphate (SCOP) gel [7,12,16] that is considered as a precursor of hydroxyapatite. A small weight loss event at around 300 °C may indicate a presence of AH<sub>3</sub> or C<sub>3</sub>AH<sub>6</sub>, suggesting that the conventional hydration of CAC might have occurred in minor amount. A similar weight loss event in TG data has been previously reported, attributing to the presence of AH<sub>3</sub> [16]. The weight loss below 150 °C was enhanced in CAP<sub>20A</sub>, indicating the interaction with the leachate

and associated hydration during the leaching test similar to the CAC system.

The weight loss observed below 150 °C was much less in CAP<sub>90</sub> compared with CAP<sub>20</sub>, meaning that majority of free water was removed in CAP<sub>90</sub> through the thermal treatment, together with some of water associated with the amorphous SCOP gel. The weight loss peak observed in the DTG curve at 100 – 200°C is likely corresponding to free water and/or the crystalline water remained with amorphous gel phase [11, 13, 16]. No observable weight loss peak at 220 – 330 °C confirms that the conventional hydration of CAC clinker phases did not take place CAP<sub>90</sub>. When CAP<sub>90</sub> is subjected to the leaching test, as shown in the DTC curve of CAP<sub>90A</sub>, only small increase in the weight loss was observed in the low temperature region from 40 – 100 °C, suggesting the increase in free water. The results show that 91 days of leaching test does not cause any observable phase evolution but only influences on the free water incorporation in the CAP system.

### 3.6. Confirmation of phases by ATR/FT-IR

**Figure 9** shows the ATR-FT/IR spectra for the CAC and CAP. The IR spectra for the CAC had very similar spectra among them regardless the curing temperature and leaching test. The bands located at 1020 cm<sup>-1</sup> and 980 cm<sup>-1</sup> in **Figure 9 (a)** correspond to δ O-H in gibbsite AH<sub>3</sub>. The strong band located at approx. 545 cm<sup>-1</sup> is associated with the ν Al-O in hydrogarnet C<sub>3</sub>AH<sub>6</sub> [28]. These are stable hydration products of the CAC clinker phases, and their formation is favored in higher temperatures [24]. Accordingly, these absorption bands are more prominent in CAC<sub>90</sub> series than in CAC<sub>20</sub> series. Absorption bands in the range of 900 – 700 cm<sup>-1</sup> are associated with Al-O vibrations in tetrahedral AlO<sub>4</sub> groups, whereas bands in the range of 680 – 500 cm<sup>-1</sup> are associated with Al-O vibrations in octahedral AlO<sub>6</sub> groups [29]. The CAC<sub>90</sub> series clearly indicates a broad absorption band in the range of 900 – 700 cm<sup>-1</sup>, suggesting the presence of tetrahedral AlO<sub>4</sub> groups. A part of this may be attributed to C<sub>2</sub>AH<sub>8</sub> [30] as identified in the XRD data, but there must be other phase(s) present in the system with AlO<sub>4</sub> groups as this peak is more prominent prior to the leaching test. On the other hand, CAH<sub>10</sub> identified in the XRD data of CAC<sub>20</sub> series has both Al(V) and Al(VI) coordination [31], and thus, it must be contributing to the absorption in the range of 680 – 500 cm<sup>-1</sup>.

With respect to the CAP systems, a strong absorption peak was observed at ~ 1024 cm<sup>-1</sup>, which must be corresponding to orthophosphate (R-PO<sub>4</sub>) [7,12,16]. Orthophosphates can show strong and broad peaks ranging from 1150 cm<sup>-1</sup> to 1000 cm<sup>-1</sup> [28, 32, 33]. These bands also coincide with the formation of SCOP gel as reported [7]. The data confirms that the sodium polyphosphate used in the CAP system was consumed by acid-base reaction, and orthophosphate gel was formed both in CAP<sub>20</sub> and CAP<sub>90</sub>.

The CAP<sub>20</sub> series clearly show additional absorption at 1080 cm<sup>-1</sup> and 910 cm<sup>-1</sup>, corresponding to ν P-O and H<sub>2</sub>PO<sub>4</sub><sup>-</sup>, respectively. These absorption band did not show obvious change in CAP<sub>20A</sub>, consistent with the general observation in the XRD and TG analysis. For the CAP<sub>90</sub> series, the main

absorption at  $\sim 1024\text{ cm}^{-1}$  corresponding to  $\text{R-PO}_4$  appear to be more intense in  $\text{CAP}_{90\text{A}}$ , possibly indicating further interaction between CAC clinker phases and phosphate that remained in the system without reacting when the samples were synthesized. Differing from the  $\text{CAP}_{20}$  series, the band at  $910\text{ cm}^{-1}$  corresponding to  $\text{H}_2\text{PO}_4^-$  was not prominent in the  $\text{CAP}_{90}$  series, but a slight increase is observable when it was subjected to the leaching test (in  $\text{CAP}_{90\text{A}}$ ). This indicates that this particular absorption band represent the water loosely bonded with the amorphous sodium calcium orthophosphate (SCOP) gel, as suggested by the TG analysis.

### *3.7. Immobilization of Sr and Cl in CAP system*

The obtained data demonstrates a great potential of CAP cement as the cementing matrix for immobilization of Sr. However, the amorphous nature of the binding phase makes it challenging to fully understand this system and how Sr is immobilized. The present study confirms the presence of amorphous orthophosphate(s) (Figure 9). The features of phosphate phases such as  $\text{NaCaPO}_4 \cdot x\text{H}_2\text{O}$  (SCOP salt [7]) and  $\text{Ca}(\text{HPO}_4) \cdot x\text{H}_2\text{O}$  (dibasic calcium phosphate [34]) match with the data obtained in the present study and our previous study [16]. Under suitable conditions, these phases can evolve to  $\text{Ca}_{10}(\text{PO}_4)_6(\text{OH})_2$  (hydroxyapatite) [7, 35] which also has features match with the data obtained. It is possible that these phases coexist in the CAP system.

Microstructural observation, in particular Energy-Dispersive X-ray spectroscopy (EDX) mapping could be usually beneficial to identify the phases responsible for the immobilization of the  $\text{Sr}^{2+}$ . Unfortunately, Sr has a similar energy in its characteristic X-ray ( $L_\alpha$  for Sr: 1.806 keV) to that of Si ( $K_\alpha$  for Si: 1.739 keV), and thus, their peaks overlap in the EDX spectrum. Considering the significant  $\text{SiO}_2$  content of approximately 6.0 wt% in Secar<sup>®</sup>51 and the small Sr content of approximately 1.7 wt% in the sample, mapping Sr using EDX would be difficult without including Si. In fact, a clear mapping of Sr in the CAP sample was difficult even in the CAP system with a reduced  $\text{SiO}_2$  (0.8 wt%) content [36] although general distribution of Sr in the binding phase was observed. For the identification of phase for Sr immobilization, it may be necessary to prepare CAP system without  $\text{SiO}_2$ .

Although the phase(s) responsible for the immobilization of  $\text{Sr}^{2+}$  in the CAP system was not directly identified, they are likely incorporated in the amorphous binding phase(s). Precipitation of hydroxyapatite with substitution of Ca by Sr has been reported in the similar alkaline aqueous environments with a complete compositional range from  $\text{Ca}_{10}(\text{PO}_4)_6(\text{OH})_2$  to  $\text{Sr}_{10}(\text{PO}_4)_6(\text{OH})_2$  [37-41]. The amorphous SCOP gel phase in the matrix may also incorporate  $\text{Sr}^{2+}$  ions, as formation of  $\text{NaSrPO}_4$  is also reported [42]. On the other hand, the leaching of  $\text{Cl}^-$  ions was significantly higher in the obtained data. As previously mentioned, apatite family of calcium phosphates is known to be a good host for halogens, and  $\text{Cl}^-$  ions can be incorporated by substituting  $\text{OH}^-$  ions. However, it has been reported that the higher the  $\text{Cl}^-$  ion incorporation, the higher the dissolution of the constituent elements of apatite [43]. A recent study [44] also shows that the co-substitution of  $\text{OH}^-$  with  $\text{Cl}^-$  and  $\text{Ca}^{2+}$  with

$\text{Na}^+$  ions caused various point defects in hydroxyapatite (e.g., negatively charged Na in Ca site, positively charged O in phosphate site, OH–Cl bonds, and a partially ‘head-on’ HO:OH structure in an hydroxyl configuration), making the system energetically less stable and consequently higher dissolution behavior in the aqueous system. Although the binding phase of the present CAC system is not well-crystalline hydroxyapatite, the aforementioned orthophosphate phases are considered to be precursor of hydroxyapatite, and thus,  $\text{Cl}^-$  ions may have a similar behavior and impact on the dissolution of the material.

The positive impact of the thermal treatment on the immobilization of  $\text{Cl}^-$  ions, observed in the present study, is likely not the fundamental change in the binding phase but the improvement in the microstructure of the material. As shown in **Figure 10** [16], thermal treatment of CAP system usually results in reduction of micro cracks [16, 36].

#### 4. Conclusions

The present study investigated the solidification and stabilization of  $\text{Sr}^{2+}$  and  $\text{Cl}^-$  in the CAC or CAP cured at 90 °C in an open system in comparison with those cured at 20 °C in a closed system. The curing period was 7 days, and then the leaching was carried out based on ANSI/ANS 16.1 up to 91 days. Findings in this study are summarized as the following:

- 1) Both the CAC and CAP systems could be solidified, using  $\text{SrCl}_2$  solution, in closed system at 20 °C and in open system at 90 °C. By a 7day curing with thermal treatment, the water content in the CAC sample was reduced only in the first day, but in the CAP sample it could be reduced down to ~40 wt%.
- 2) In the leaching test, a metastable phase ( $\text{C}_2\text{AH}_8$ ) was formed in the  $\text{CAC}_{90}$ , but no crystalline phase was formed in the  $\text{CAC}_{20}$ ,  $\text{CAP}_{20}$  and the  $\text{CAP}_{90}$ . Interaction with the leachate was observed in the all systems investigated, resulting in the increase in the amorphous gel phases and/or hydration of remaining CAC clinkers.
- 3)  $\text{Sr}^{2+}$  could be stabilized in the  $\text{CAP}_{20}$  and the  $\text{CAP}_{90}$  more effectively than in the  $\text{CAC}_{20}$  and the  $\text{CAC}_{90}$ . It was expected that  $\text{Sr}^{2+}$  existed in insoluble amorphous gel. The  $\text{Sr}^{2+}$  immobilization became slightly better in the thermally treated samples in both CAC and CAP.
- 4) The CAC system could stabilize  $\text{Cl}^-$  ions in Friedel’s salt, which appears to be effective for the immobilization of  $\text{Cl}^-$ . The stabilization of  $\text{Cl}^-$  ions in the CAP system was improved by thermal treatment. An incorporation of  $\text{Cl}^-$  in poorly crystalline hydroxyapatite may be a possible explanation.

The reduction of water content and the stabilization of Sr<sup>2+</sup> ion in the CAP<sub>90</sub> were the most effective in the present study. This result would be beneficial to prevent the risks of fire and explosion due to the accumulation of radiolysis H<sub>2</sub> gas, and to mitigate potential risks of leakage into the environment. However, with respect to the stabilization of Cl<sup>-</sup> ion, Friedel's salt in the CAC was more effective. The stabilization of Cl<sup>-</sup> ion would be improved by further enhancing the apatite formation in the CAP system.

### Acknowledgements

This work was supported by MEXT Nuclear Energy S&T and Human Resource Development Project through concentrating wisdom Grant Number JPMX 15D15658389 and the Engineering and Physical Science Research Council, UK (EP/N017684/1). The authors thank Dr. Yoshihiro Meguro and Mr. Osamu Nakazawa for helping this collaboration research and Dr. Sujitra Onutai for fruitful comments.

### References

- [1] Y. Fukuda, Y. Arai, H. Hinai, M. Ichikawa, R. Takahashi, F. Hirayama, M. Obata, M. Akagi, T. Fukumatsu, A. Shibata, K. Nomura, "Characterization of Carbonate Slurry generated from Multiple Radio-nuclides Removal System in Fukushima Daiichi Nuclear Power Station," *Proceedings of ICAPP2017*, No. 17077, Fukui and Kyoto, April 24-28 (2017) 7 pages.
- [2] S.M.L. Hardie, I.G. McKinley, S. Lomperski, H. Kawamura, T.M. Beattie, "Management options for Fukushima corium," *Prog. Nucl. Energy*, **92** (2016) 260-266.
- [3] F.P. Glasser, "Progress in the immobilization of radioactive wastes in cement," *Cem. Concr. Res.*, **22** (1992) 201-206.
- [4] Kerneous Inc., Secar@51, Safety Data Sheet, version 1.2 (2016) 6 pages.
- [5] H. Kinoshita, P. Swift, C. Utton, B. Carro-Mate, G. Marchand, N. Collier, N. Milestone, Corrosion of aluminium metal in OPC- and CAC-based cement matrices, *Cem. Concr. Res.*, **50** (2013) 11-18.
- [6] T. Sugama, N.R. Carciello, Strength development in phosphate-bonded calcium aluminate cements, *J. Am. Ceram. Soc.*, **74**, 5 (1991) 1023-1030.

- [7] T. Sugama, N.R. Carciello, Sodium phosphate-derived calcium phosphate cements, *Cem. Concr. Res.*, **25**, 1 (1995) 91–101.
- [8] W. Ma, P.W. Brown, Mechanical behaviour and microstructural development in phosphate modified high alumina cement, *Cem. Concr. Res.*, **22** (1992) 1192–1200.
- [9] W. Ma, P.W. Brown, Hydration of sodium phosphate-modified high alumina cement, *J. Mater. Res.*, **9**, 5 (1994) 1291–1297.
- [10] M.A. Chavda, H. Kinoshita, J.L. Provis, Phosphate modification of calcium aluminate cement to enhance stability for immobilisation of metallic wastes, *Adv. Appl. Ceram.*, **113** (2014) 453-459.
- [11] M.A. Chavda, S.A. Bernal, D.C. Apperley, H. Kinoshita, J.L. Provis, Identification of the hydrate gel phases present in phosphate-modified calcium aluminate binders, *Cem. Concr. Res.*, **70** (2015) 21-28.
- [12] K. Irisawa, I. Garcia-Lodeiro, H. Kinoshita, Influence of mixing solution on characteristics of calcium aluminate cement modified with sodium polyphosphate, *Cem. Concr. Res.*, **128** (2020) 10591.
- [13] P.D. Swift, H. Kinoshita, N.C. Collier, C.A. Utton, Phosphate-modified calcium aluminate cement for radioactive waste encapsulation, *Adv. Appl. Ceram.*, **112** (2013) 1-8.
- [14] J.M. Fernandez, I. Navarro-Blasco, A. Duran, R. Sirera, J.I. Alvarez, Treatment of toxic metal aqueous solutions: encapsulation in a phosphate-calcium aluminate matrix, *J. Environ. Manag.*, **140** (2014) 1-13.
- [15] I. Navarro-Blasco, A. Duran, M. Perez-Nicolas, J.M. Fernandez, R. Sirera, J.I. Alvarez, A safe disposal phosphate coating sludge by formation of an amorphous calcium phosphate matrix, *J. Environ. Manag.*, **159** (2015) 288-300.
- [16] I. Garcia-Lodeiro, K. Irisawa, F. Jin, Y. Meguro, H. Kinoshita, Reduction of water content in calcium aluminate cement with/out phosphate modification for alternative cementation technique, *Cem. Concr. Res.*, **109** (2018) 243-253.
- [17] S. Kamaluddin, I. Garcia-Lodeiro, H. Kinoshita, Strontium in phosphate-modified calcium aluminate cement, *Key Eng. Mater.*, **803** (2019) 341-345.

- [18] H. Kinoshita, "Chapter 10 Development of ceramic matrices." in: M. I. Ojovan, Ed., *Handbook of Advanced Radioactive Waste Conditioning Technology*, Woodhead, Cambridge UK (2011) 293-338.
- [19] T. M Rosseel, I. Maruyama, Y. Le Pape, O. Kontani, A. B. Giorla, I. Remec, J. J. Wall, M. Sircar, C. Andrade and M. Ordonez, "Review of the current state of knowledge on the effects of radiation on concrete." *Journal of Advanced Concrete Technology*, 14 (2016) 368-383.
- [20] American Nuclear Society, Measurement of the leachability of solidified low-level radioactive wastes by a short-term test procedure, ANSI/ANS-16.1 (1986).
- [21] H. Matsuzuru, A. Ito, Leaching behavior of strontium-90 in cement composites, *Ann. Nucl. Energy*, **4** (1977) 465-470.
- [22] A.M. El-Kamash, M.R. El-Naggar, M.I. El-Dessouky, Immobilization of cesium and strontium radionuclides in zeolite-cement blends, *J. Hazard. Mater.*, **B136** (2006) 310-316.
- [23] R.O. Abdel Rahman, D.H.A. Zin El Abidin, H. Abou-Shady, Assessment of strontium immobilization in cement-bentonite matrices, *Chem. Eng. J.*, **228** (2013) 772-780.
- [24] V. Antonovic, J. Keriene, R. Boris, M. Aleknevicius, The effect of temperature on the formation of the hydrated calcium aluminate cement structure, *Procedia Eng.*, **57** (2013) 99-106.
- [25] R. Ito, G. Dodbiba, T. Fujita, J.W. Ahn, Removal of insoluble chloride from bottom ash for recycling, *Waste Manage.*, **28** (2008) 1317-1323.
- [26] S.M. Bushnell-Watson, J.H. Sharp, The application of thermal analysis to the hydration and conversion Reactions of calcium aluminate Cement, *Materials de Construction*, **42**, 228 (1992) 13-32.
- [27] V. Balek, J. Subrt, J. Rouquerol, P. Llewlllyn, V. Zelenak, I.M. Bountsewa, I.N. Beckman, K. Gyoryova, Emanation thermal analysis study of synthetic gibbsite, *J. Therm. Anal. Calorim.*, **71** (2003) 773-782.
- [28] A. Hidalgo, J.L. Carcia, M.C. Alonso, L. Fernandez, C. Andrade, Microstructure development in mixes of calcium aluminate cement with silica fume or fly ash, *J. Therm. Anal. Calorim.*, **96**, 2 (2009) 335-345.

- [29] P. Tarte, Infra-red spectra of inorganic aluminates and characteristic vibrational frequencies of  $\text{AlO}_4$  tetrahedra and  $\text{AlO}_6$ , *Spectrochim. Acta*, **23A** (1967) 2127-2087.
- [30] G. Geng, J. Li, Y.S. Yu, D.A. Shapiro, D.A.L. Kilcoyne, P.J.M. Monteiro, Nanometer-resolved spectroscopic study reveals the conversion mechanism of  $\text{CaO} \cdot \text{Al}_2\text{O}_3 \cdot 10\text{H}_2\text{O}$  to  $2\text{CaO} \cdot \text{Al}_2\text{O}_3 \cdot 8\text{H}_2\text{O}$  and  $3\text{CaO} \cdot \text{Al}_2\text{O}_3 \cdot 6\text{H}_2\text{O}$  at an elevated temperature, *Cryst. Growth Des.*, **17** (2017) 4246-4253.
- [31] A.N. Christensen, T.R. Jensen, B. Lebech, J.C. Hanson, H.J. Jakobsen, J. Skibsted, Thermal decomposition of monocalcium aluminate decahydrate ( $\text{CaAl}_2\text{O}_4 \cdot 10\text{H}_2\text{O}$ ) investigated by *in-situ* synchrotron X-ray powder diffraction, thermal analysis and  $^{27}\text{Al}$ ,  $^2\text{H}$  MAS NMR spectroscopy, *Dalton Trans.*, **455** (2008) 455-462.
- [32] T. Sugama, M. Allan, J.M. Allan, Calcium phosphate cements prepared by acid-base reaction, *J. Am. Ceram. Soc.*, **75**, 8 (1992) 2076-2087.
- [33] Y.M. Moustafa, K. El-Egili, Infrared spectra of sodium phosphate glasses, *J. Non-Cryst. Solids*, **240** (1998) 144-153.
- [34] T. Sugama, L.E. Brothers, L. Weber, Calcium aluminate cements in fly ash/calcium aluminate blend phosphate cement systems: their role in inhibiting carbonation and acid corrosion at low hydrothermal temperature of  $90^\circ\text{C}$ , *J. Mater. Sci.*, **37** (2002) 3163-3173.
- [35] T. Sugama, J.M. Hill, Calcium phosphate cements prepared by acid-base reaction, *J. Am. Ceram. Soc.*, **75**, 8 (1992) 2076-2087.
- [36] H. Mohammed, I. Garcia-Lodeiro, H. Kinoshita, Modification of Calcium Aluminate Cement with Phosphate for Incorporation of Strontium Chloride, *J. Adv. Concr. Technol.*, **19** (2021) 1296-1308.
- [37] X. Wang, J. Ye, Variation of crystal structure of hydroxyapatite in calcium phosphate cement by the substitution of strontium ions, *J. Mater. Sci: Mater Med.*, **19** (2008) 1183-1186.

- [38] M. Kikuchi, A. Yamazaki, R. Otsuka, M. Akao, H. Aoki, Crystal structure of Sr-substituted hydroxyapatite synthesized by hydrothermal method, *J. Solid State Chem.*, **13**, 2 (1994) 373-378.
- [39] C.J. Harrison, P.V. Hatton, P. Gentile, C.A. Miller, Nanoscale strontium-substituted hydroxyapatite pastes and gels for bone tissue regeneration, *Nanomaterials*, **11** (2021) 1611.
- [40] M. Frasnelli, F. Cristofaro, V.M. Sglavo, S. Dirè, E. Callone, R. Ceccato, G. Bruni, A.I. Cornaglia, L. Visai, Synthesis and characterization of strontium-substituted hydroxyapatite nanoparticles for bone regeneration, *Mater. Sci. Eng. C*, **71** (2017) 653–662.
- [41] M.P. Đorđević, J. Maletaškić, N. Stanković, B. Babić, K. Yoshida, T. Yano, B. Matović, In-situ immobilization of Sr radioactive isotope using nanocrystalline hydroxyapatite, *Ceram. Int.*, **44** (2018) 1771–1777.
- [42] E.D. Byzova, A.B. Ivanov, V.A. Volkovich, A.V. Chukin, Strontium phosphates precipitation from alkali chloride based melts, *AIP Conference Proceedings*, **2313** (2020) 050008.
- [43] J.S. Cho, D.S. Yoo, Y.-C. Chung, S.-H. Rhee, Enhanced bioactivity and osteoconductivity of hydroxyapatite through chloride substitution, *J. Biomed Mater. Res. Part A*, **102**, 2 (2014) 455–469.
- [44] D.S. Yoo, J.S. Cho, Y.-C. Chung, S.-H. Rhee, Defect structures of sodium and chloride co-substituted hydroxyapatite and its osseointegration capacity, *J. Mater. Sci.*, **56** (2021) 5493–5508.

## Figure captions

- Figure 1. Remaining water contents (wt%) in CAC<sub>20</sub> (○), CAC<sub>90</sub> (●), CAP<sub>20</sub> (□) and CAP<sub>90</sub> (■) during the initial 7 days of curing.
- Figure 2. CFL of Sr<sup>2+</sup> in CAC<sub>20</sub> (○), CAC<sub>90</sub> (●), CAP<sub>20</sub> (□) and CAP<sub>90</sub> (■) against time (days).
- Figure 3. CFL of Sr<sup>2+</sup> in (a) CAC<sub>20</sub> (○), CAC<sub>90</sub> (●) and (b) CAP<sub>20</sub> (□), CAP<sub>90</sub> (■) against square root of time (s<sup>1/2</sup>).
- Figure 4. CFL of Cl<sup>-</sup> in CAC<sub>20</sub> (○), CAC<sub>90</sub> (●), CAP<sub>20</sub> (□) and CAP<sub>90</sub> (■) against time (days).
- Figure 5. CFL of Cl<sup>-</sup> in CAC<sub>20</sub> (○), CAC<sub>90</sub> (●), CAP<sub>20</sub> (□) and CAP<sub>90</sub> (■) against square root of time (s<sup>1/2</sup>).
- Figure 6. X-ray diffractograms for CAC and CAP systems (a) prior and (b) subsequent to the leaching test. m: monocalcium aluminate, g: gehlenite, p: perovskite, D: monocalcium aluminate decahydrate, O: dicalcium aluminate octahydrate, H: hydrogarnet, F: Friedel's salt.
- Figure 7. (a) Thermogravimetry (TG) and (b) derivative thermogravimetry (DTG) for the CAC system against temperature.
- Figure 8. (a) Thermogravimetry (TG) and (b) derivative thermogravimetry (DTG) for the CAP system against temperature.
- Figure 9. ATR-FT/IR spectra for (a) the CAC and (b) the CAP systems.
- Figure 10. Effect of thermal treatment on the microstructure of CAP system obtained by Garcia-Lodeiro et al. [16]: (a) cured at 35 °C and (b) cured at 95 °C.

## Table titles

Table 1. Analysis of leaching results for CAC and CAP samples

Sample	S/V ratio (m <sup>-1</sup> )	CFL/√t		R <sup>2</sup>		D <sub>e</sub> (m <sup>2</sup> /s)	
		Sr <sup>2+</sup>	Cl <sup>-</sup>	Sr <sup>2+</sup>	Cl <sup>-</sup>	Sr <sup>2+</sup>	Cl <sup>-</sup>
CAC <sub>20</sub>	0.00279	6 × 10 <sup>-5</sup>	5 × 10 <sup>-5</sup>	0.997	0.998	2 × 10 <sup>-14</sup>	2 × 10 <sup>-14</sup>
CAC <sub>90</sub>	0.00282	4 × 10 <sup>-5</sup>	2 × 10 <sup>-4</sup>	0.996	0.989	1 × 10 <sup>-14</sup>	3 × 10 <sup>-13</sup>
CAP <sub>20</sub>	0.00279	3 × 10 <sup>-7</sup>	6 × 10 <sup>-4</sup>	0.985	0.999	5 × 10 <sup>-19</sup>	2 × 10 <sup>-12</sup>
CAP <sub>90</sub>	0.00273	2 × 10 <sup>-7</sup>	3 × 10 <sup>-4</sup>	0.971	0.999	2 × 10 <sup>-19</sup>	5 × 10 <sup>-13</sup>

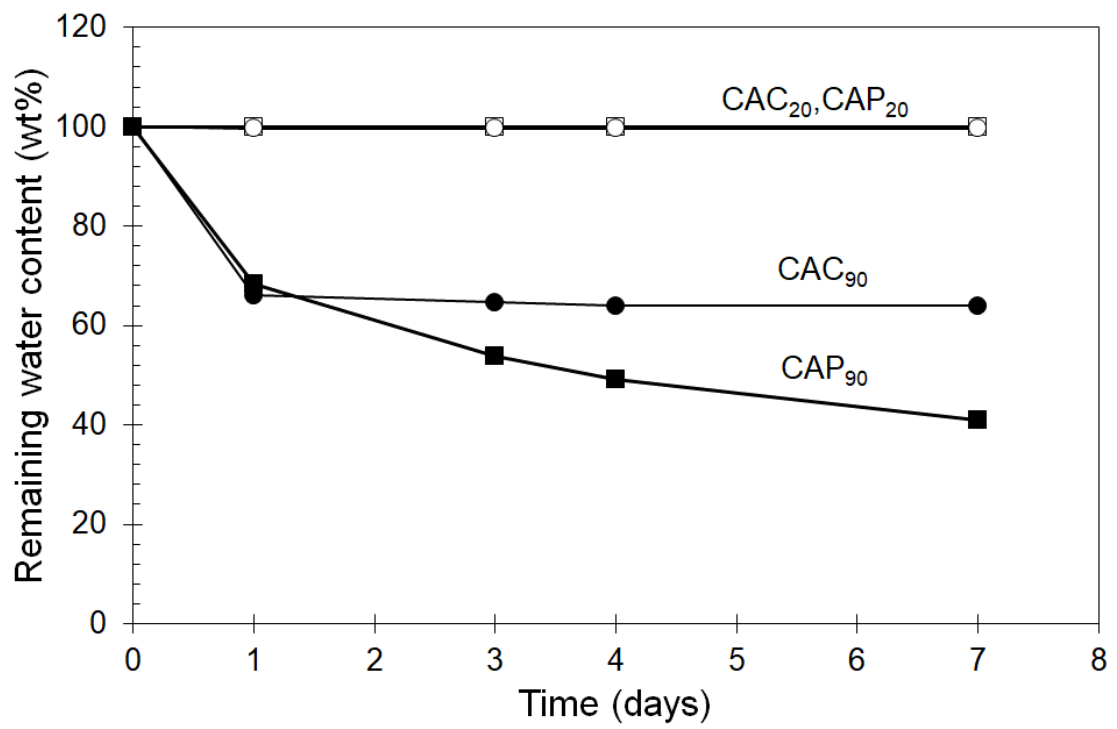


Figure 1. Remaining water contents (wt%) in CAC<sub>20</sub> (○), CAC<sub>90</sub> (●), CAP<sub>20</sub> (□) and CAP<sub>90</sub> (■) during the initial 7 days of curing.

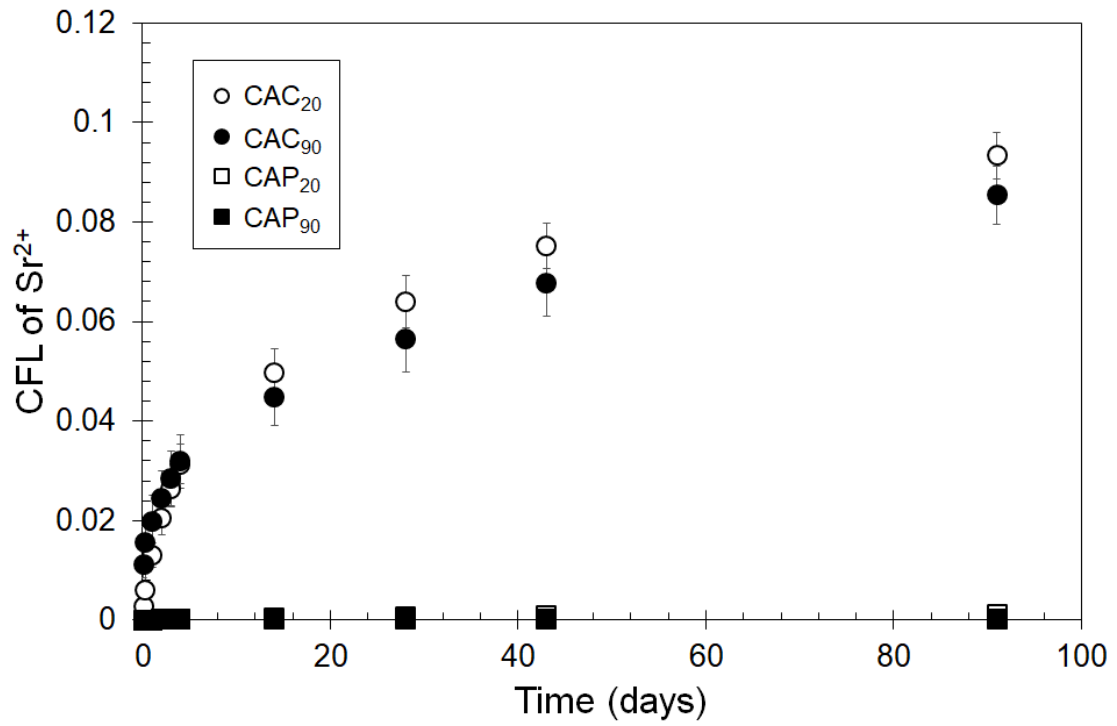


Figure 2. CFL of Sr<sup>2+</sup> in CAC<sub>20</sub> (○), CAC<sub>90</sub> (●), CAP<sub>20</sub> (□) and CAP<sub>90</sub> (■) against time (days).

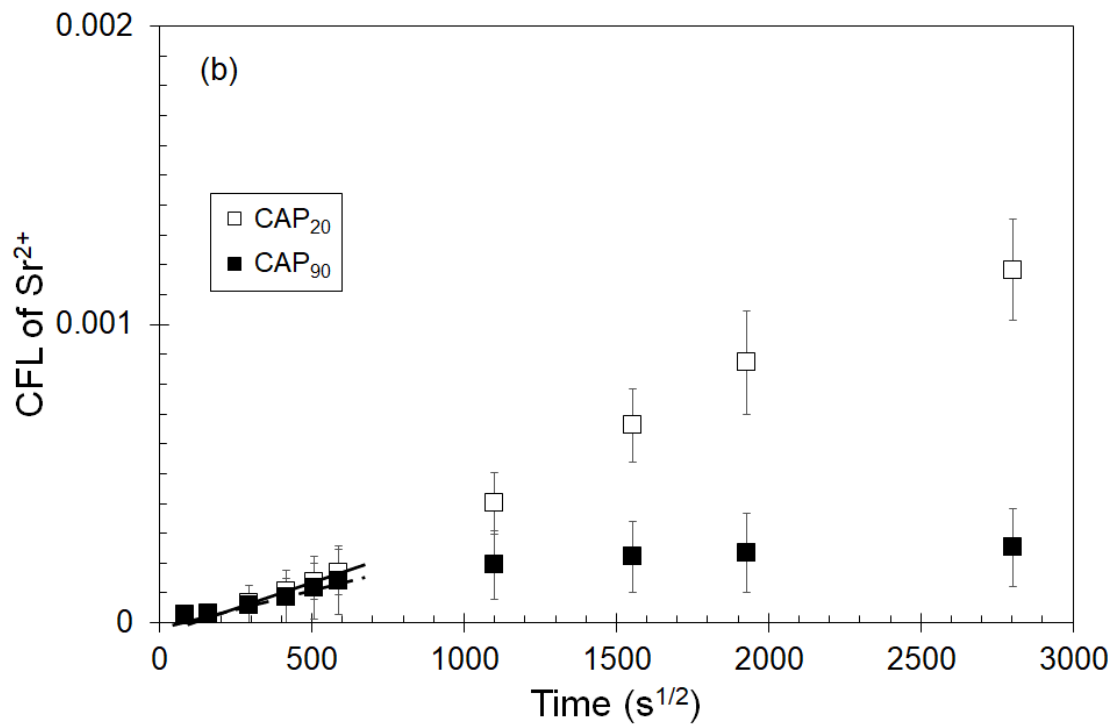
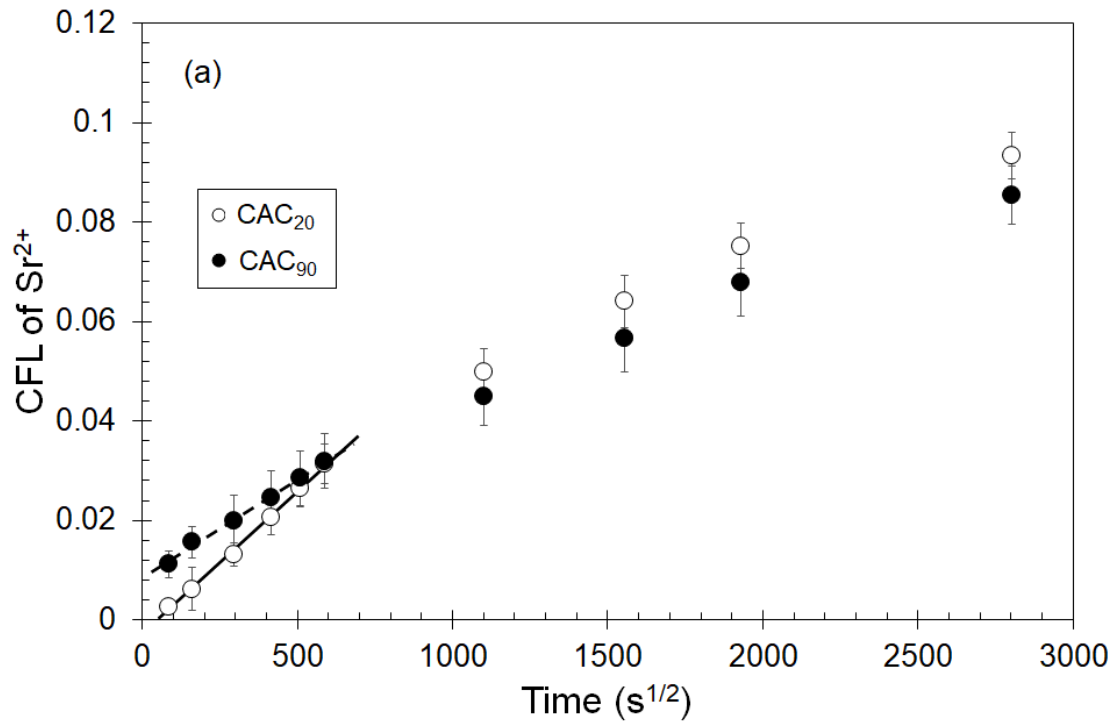


Figure 3. CFL of  $\text{Sr}^{2+}$  in (a) CAC<sub>20</sub> ( $\circ$ ), CAC<sub>90</sub> ( $\bullet$ ) and (b) CAP<sub>20</sub> ( $\square$ ), CAP<sub>90</sub> ( $\blacksquare$ ) against square root of time ( $\text{s}^{1/2}$ ).

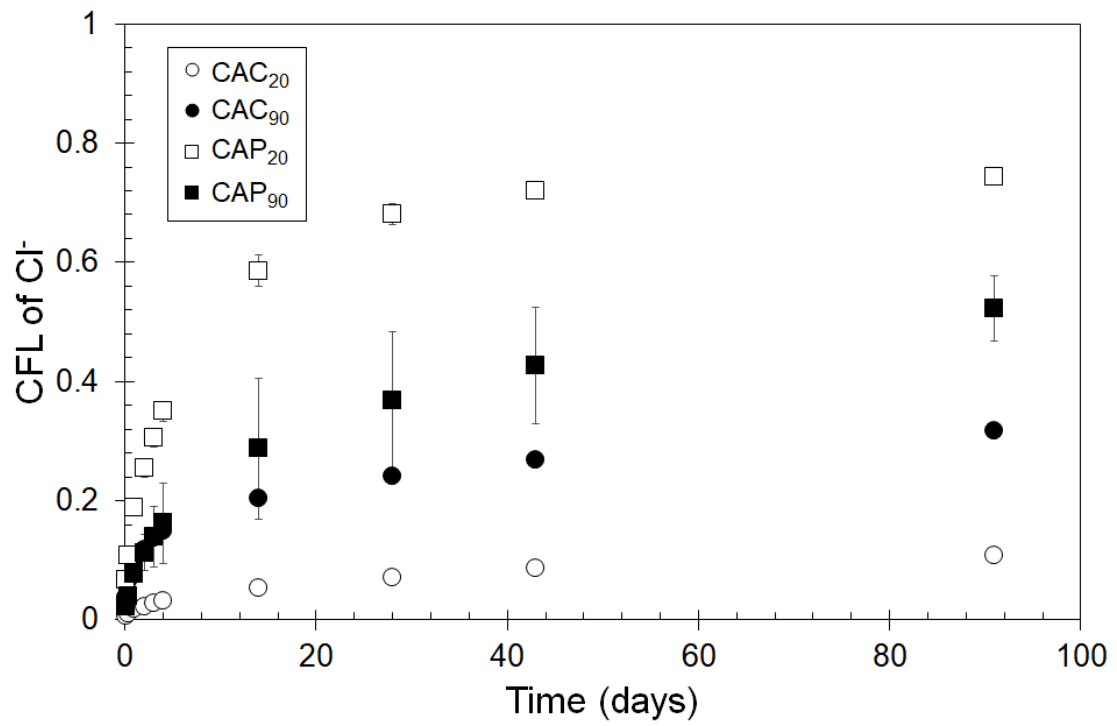


Figure 4. CFL of Cl<sup>-</sup> in CAC<sub>20</sub> (○), CAC<sub>90</sub> (●), CAP<sub>20</sub> (□) and CAP<sub>90</sub> (■) against time (days).

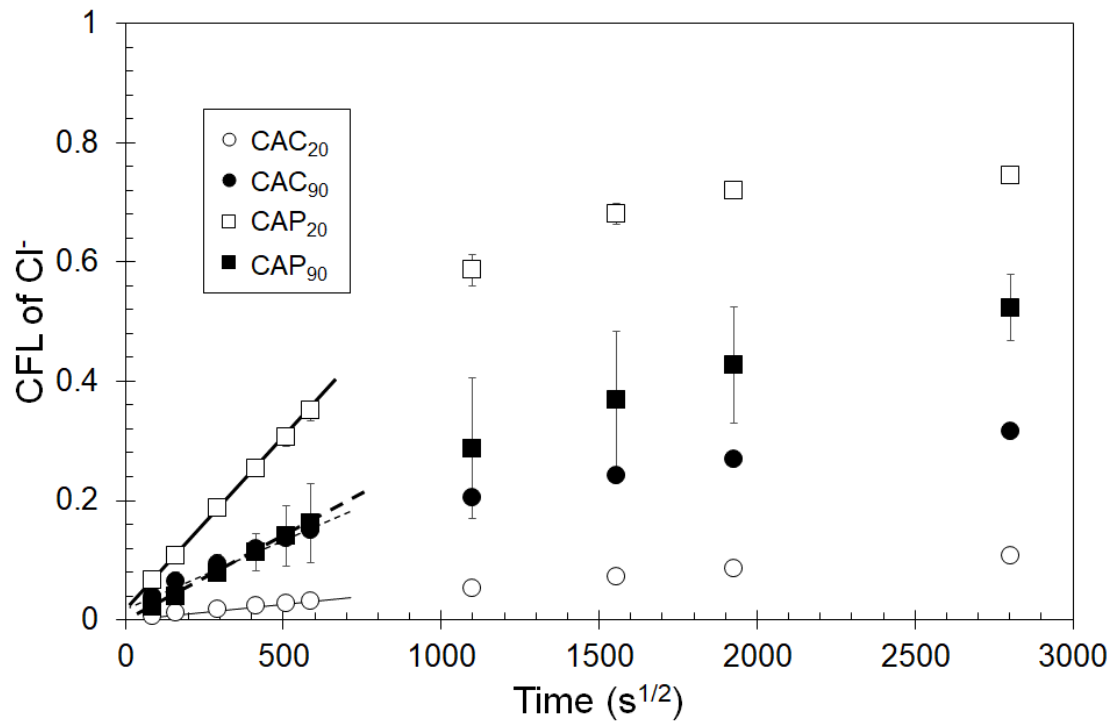


Figure 5. CFL of  $\text{Cl}^-$  in  $\text{CAC}_{20}$  (○),  $\text{CAC}_{90}$  (●),  $\text{CAP}_{20}$  (□) and  $\text{CAP}_{90}$  (■) against square root of time ( $\text{s}^{1/2}$ ).

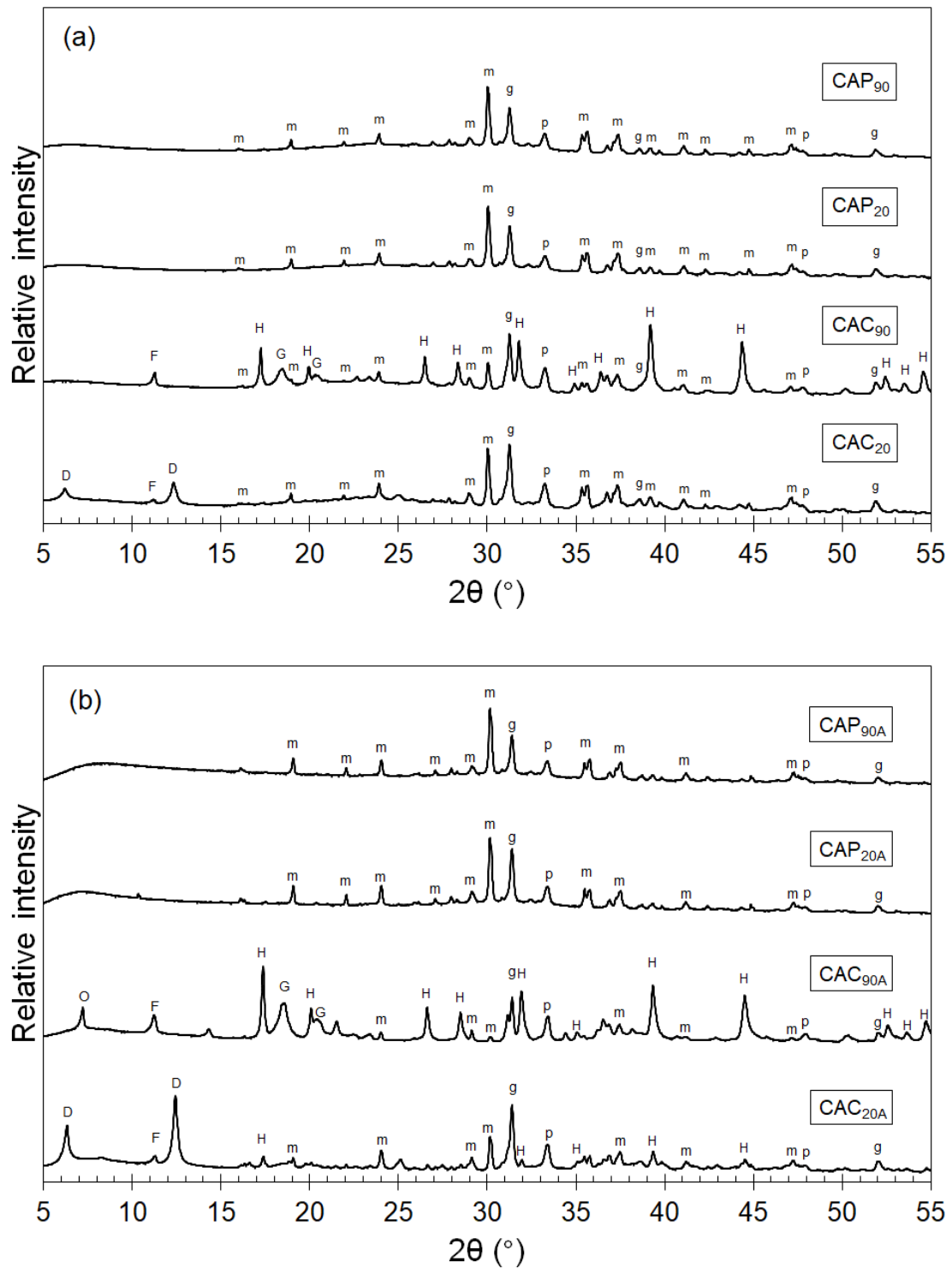


Figure 6. X-ray diffractograms for CAC and CAP systems (a) prior and (b) subsequent to the leaching test. m: monocalcium aluminate, g: gehlenite, p: perovskite, D: monocalcium aluminate decahydrate, O: dicalcium aluminate octahydrate, H: hydrogarnet, F: Friedel's salt.

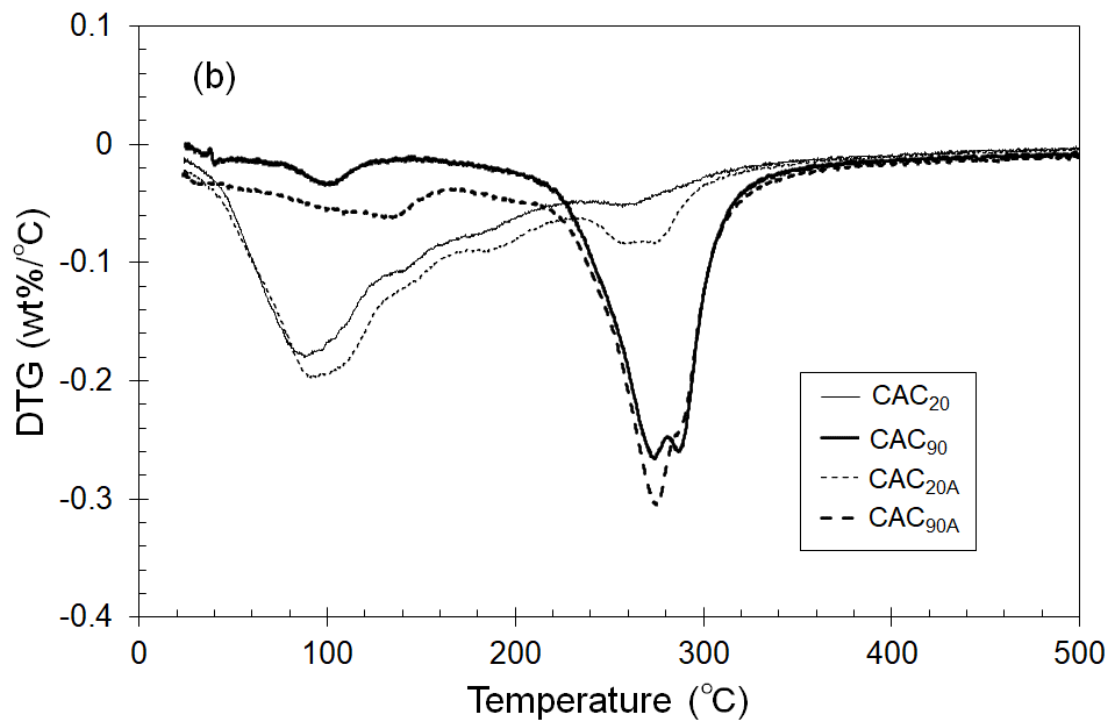
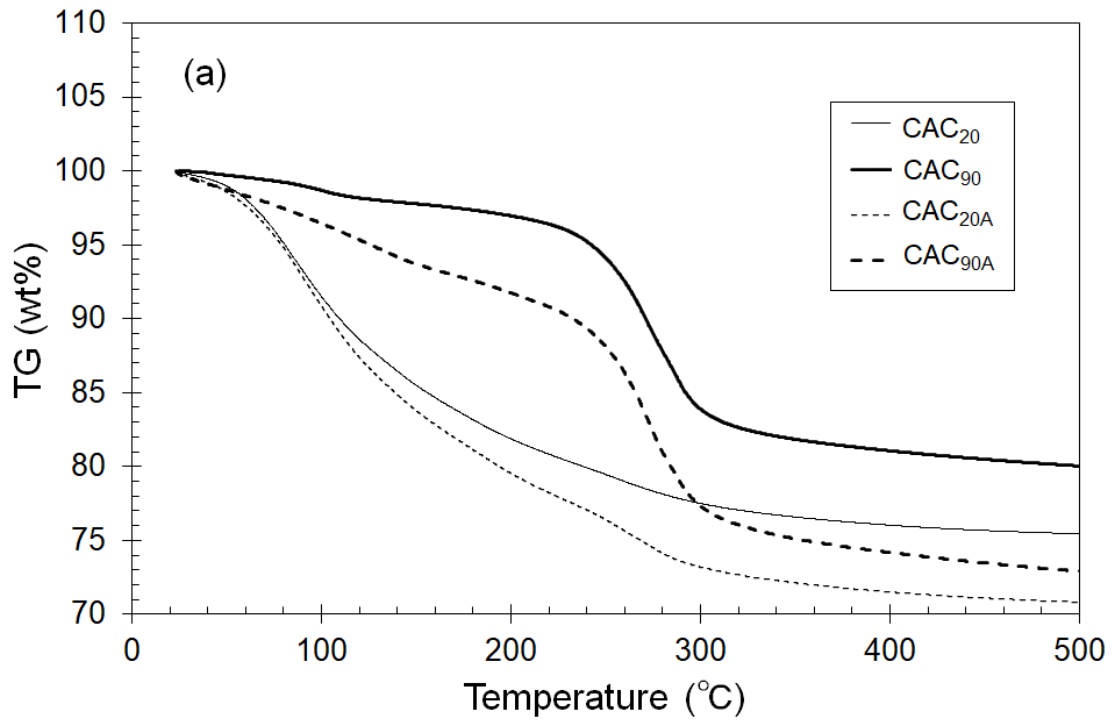


Figure 7. (a) Thermogravimetry (TG) and (b) derivative thermogravimetry (DTG) for the CAC system against temperature.

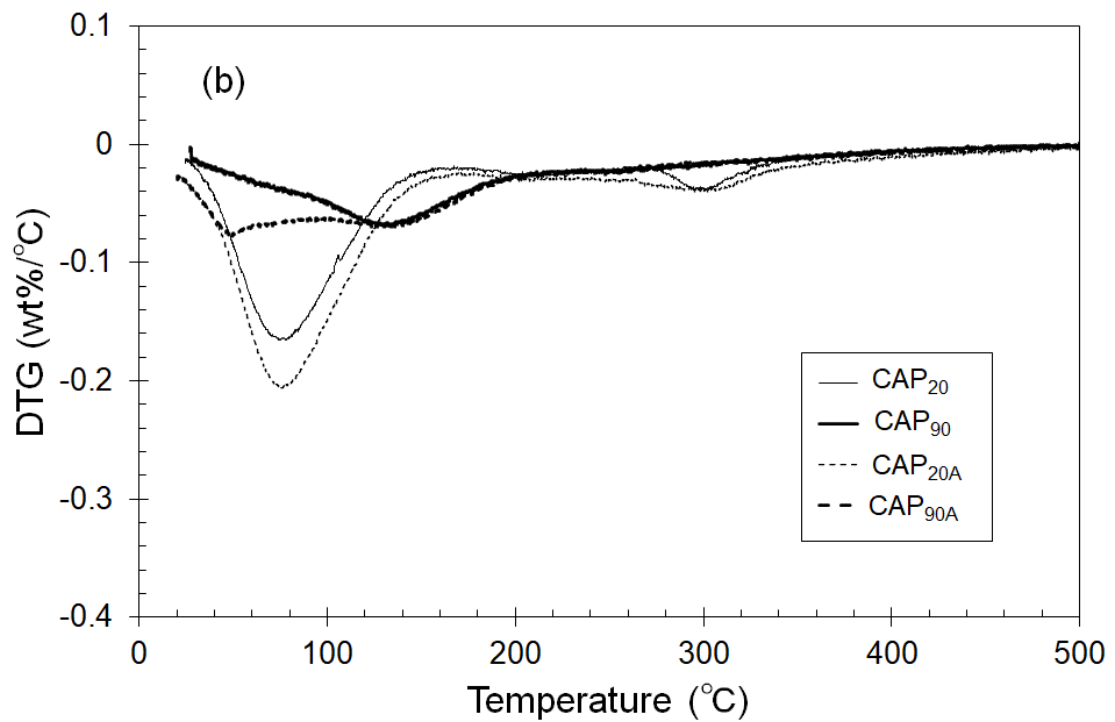
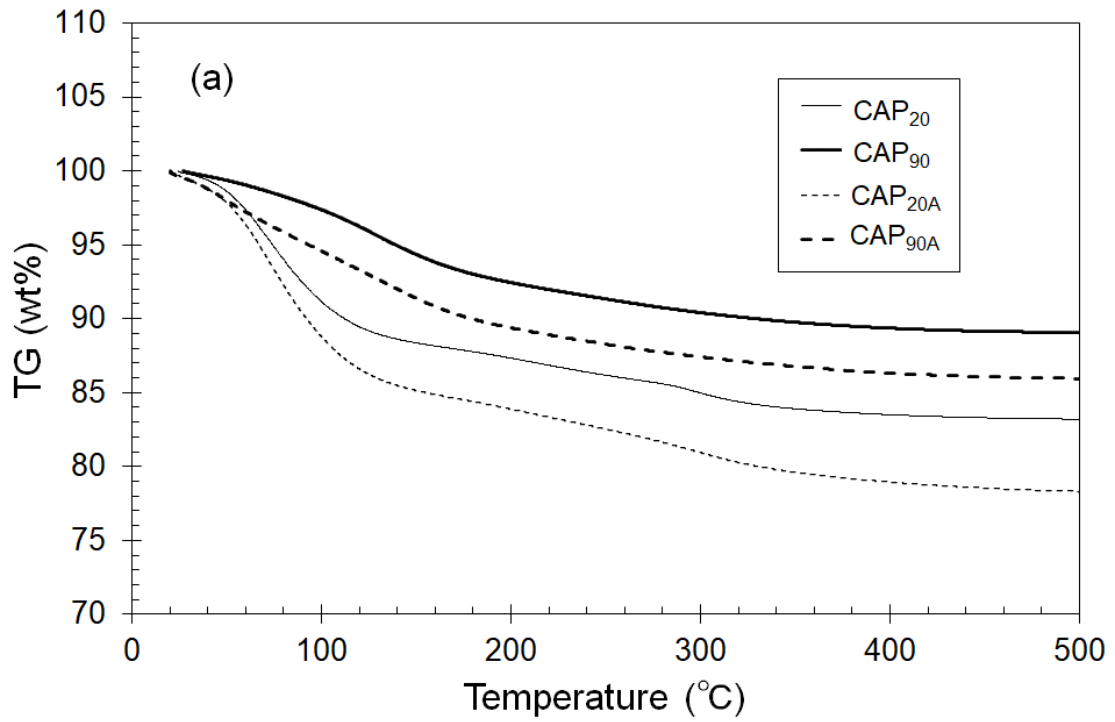


Figure 8. (a) Thermogravimetry (TG) and (b) derivative thermogravimetry (DTG) for the CAP system against temperature.

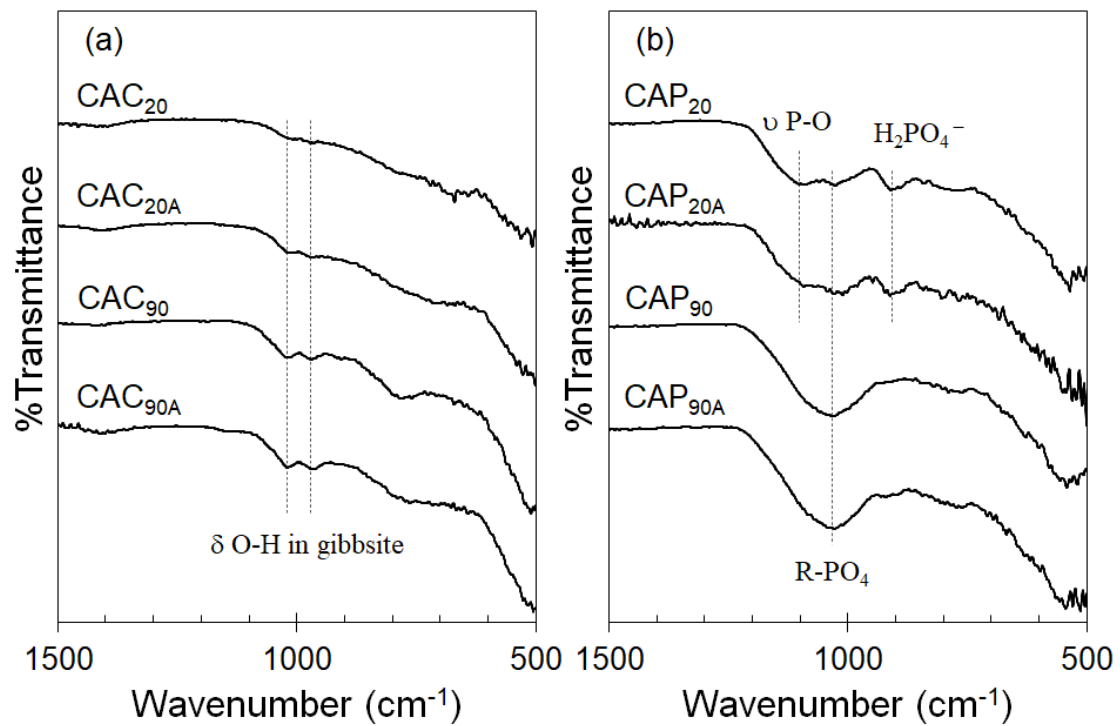


Figure 9. ATR-FT/IR spectra for (a) the CAC and (b) the CAP systems.

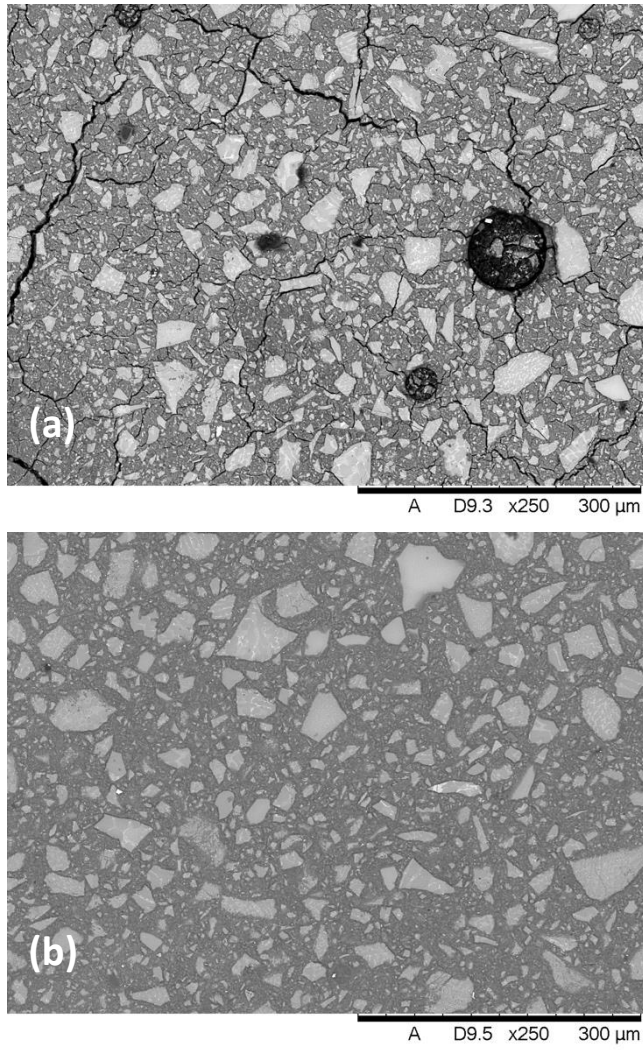


Figure 10. Effect of thermal treatment on the microstructure of CAP system obtained by Garcia-Lodeiro et al. [16]: (a) cured at 35 °C and (b) cured at 95 °C.